


Characterizing the initial- and final-state effects in isobaric collisions at energies available at the BNL Relativistic Heavy Ion Collider

Niseem Magdy ^{*}

Center for Frontiers in Nuclear Science, State University of New York, Stony Brook, New York 11794, USA
and Department of Chemistry, State University of New York, Stony Brook, New York 11794, USA

 (Received 28 September 2023; revised 28 November 2023; accepted 8 January 2024; published 7 February 2024)

A multiphase transport model (AMPT) is employed to predict symmetric correlations (SC), asymmetric correlations (ASC), normalized symmetric correlations (NSC), and normalized asymmetric correlations (NASC) in $^{96}\text{Ru} + ^{96}\text{Ru}$ and $^{96}\text{Zr} + ^{96}\text{Zr}$ collisions at 200 GeV. This study offers insights into the behavior of SC, ASC, NSC, and NASC, considering various nuclear structure scenarios to account for differences between the two isobars. Additionally, I emphasize the importance of detailed experimental measurements as they will serve as a critical constraint for refining the predictions of theoretical models.

DOI: [10.1103/PhysRevC.109.024906](https://doi.org/10.1103/PhysRevC.109.024906)

I. INTRODUCTION

The strongly coupled quark gluon plasma (QGP) is expected to be created in the nuclear collisions at the BNL Relativistic Heavy Ion Collider (RHIC) and the CERN Large Hadron Collider (LHC). A comprehensive description and understanding of the QGP transport properties (i.e., the specific viscosity η/s) is essential to the ongoing high-energy nuclear research. Nevertheless, such a description demands a detailed understanding of the heavy ion collisions (HIC) initial state [1–16]. Many studies have highlighted the importance of anisotropic flow measurements to serve as a valuable input for examining both the initial conditions and transport properties of the QGP [17–25].

Indeed, considerable research efforts have provided a rich collection of knowledge about the HIC initial conditions and the QGP properties. This valuable knowledge has been obtained by conducting extensive investigations into the n th order flow harmonics. Note that, the n th complex flow vector with Ψ_n direction and v_n magnitude is given as [26,27]

$$V_n = v_n e^{in\Psi_n}, \quad (1)$$

where v_1 , v_2 , and v_3 are the dipolar, elliptic, and triangular flow harmonics, respectively. The V_n gives the hydrodynamic response of the created medium to the n th-order initial-state eccentricity ε_n [28,29]. These studies have explored the flow harmonics magnitudes, statistical variations, fluctuations, and the correlations among them [10,16,24,29–52]. In HIC, the structure of the colliding nuclei can impact the n th order flow harmonics v_n , which reflect the initial state eccentricities ε_n dependence on the colliding nuclei structure [53–56]. Such structure can be described with the woods-Saxon distribution

for the nuclear density as

$$\rho(r, \theta, \phi) \propto \frac{1}{1 + e^{(r-R(\theta, \phi))/a_0}}, \quad (2)$$

$$R(\theta, \phi) = R_0(1 + \beta_2 Y_2^0(\theta, \phi) + \beta_3 Y_3^0(\theta, \phi)), \quad (3)$$

where $R(\theta, \phi)$ is the nuclear surface incorporating the quadrupole and octupole deformations controlled by β_2 and β_3 , respectively, the parameters R_0 and a_0 describe the half-width radius and nuclear skin thickness [57,58].

Recent theoretical and experimental studies have suggested that investigating the ratios of the n th-order flow harmonics (i.e., $\frac{v_n^{\text{Ru+Ru}}}{v_n^{\text{Zr+Zr}}}$) will provide essential insights on the structure of the colliding nuclei [56,59–76]. In the case of Ru + Ru and Zr + Zr collisions, the hope was to impose constraints on the differences in the nuclear deformation and nuclear skin between them. Building these ratios stems from the expectation that the viscosity attenuation effects in these isobaric collisions should be similar [47]. In contrast, slight variations in their deformation and nuclear skin can lead to differences in the initial-state eccentricities [53,54], causing apparent disparities in the magnitudes of v_2 and v_3 between Ru + Ru and Zr + Zr. Many of these investigations focused on the isobaric ratios only. This work highlights the value of the observables sensitive to initial and final state effects.

Reaching a comprehensive understanding of the QGP requires a simultaneous constraint on estimating the initial state eccentricities and their fluctuations and correlations as well as the final state viscous attenuation (η/s) [77,78]. In a prior investigation [16], I showed that such constraints can be achieved via data model comparisons of symmetric correlations (SC), asymmetric correlations (ASC) [79–84], normalized symmetric correlations (NSC), and normalized asymmetric correlations (NASC) [82,85–87]. Consequently, in this work, I will extend the previous study of SC, ASC, NSC, and NASC [79–82,85,86] to the Ru + Ru and Zr + Zr at RHIC top energy. In addition, I systematically investigate

^{*}niseemm@gmail.com

TABLE I. Summary of the Woods-Saxon parameters for ^{96}Ru and ^{96}Zr employed in the AMPT studies.

AMPT-set	R_0	a_0	β_2	β_3
$^{96}\text{Ru}+^{96}\text{Ru}$ (Case-1)	5.09	0.46	0.162	0.00
$^{96}\text{Zr}+^{96}\text{Zr}$ (Case-2)	5.02	0.52	0.06	0.20
$^{96}\text{Zr}+^{96}\text{Zr}$ (Case-3)	5.09	0.46	0.06	0.20
$^{96}\text{Zr}+^{96}\text{Zr}$ (Case-4)	5.09	0.46	0.06	0.00

the influence of the initial state deformation and nuclear skin using a multiphase transport (AMPT) model [88] on the SC, ASC, NSC, and NASC.

The motivation behind these investigations is to provide a systematic study of a comprehensive set of flow correlators that have the potential to constrain the HIC's initial and final effects simultaneously. In this work, I limit the presentation of the results to the system-size comparisons to provide the AMPT predictions of those flow observables. The paper is organized as follows. Section II summarizes the theoretical model used to investigate the SC, ASC, NSC, and NASC and the details of the analysis method employed. The results are presented in Sec. III followed by a summary and outlook in Sec. IV.

II. METHODOLOGY

A. The AMPT model

The current investigation employs the AMPT model to study the SC, ASC, NSC, and NASC in $^{96}\text{Ru} + ^{96}\text{Ru}$ and $^{96}\text{Zr} + ^{96}\text{Zr}$ collisions at $\sqrt{s_{NN}} = 200$ GeV. The AMPT model [88] is a comprehensive simulation framework widely utilized to delve into the complexities of relativistic heavy-ion collisions [88–95]. In this investigation, I generated AMPT events incorporating the string-melting option. Within the AMPT framework, the Glauber model defines the shape and radial distribution of the colliding nuclei, employing a deformed Woods-Saxon distribution [96] as given in Eq. (2). In AMPT simulations, the projectile and target nuclei are rotated event-by-event randomly along the polar and azimuthal directions. These analyses consider the intrinsic deformations and nuclear skin differences between ^{96}Ru and ^{96}Zr . Therefore, the Woods-Saxon parameter sets for ^{96}Ru and ^{96}Zr employed in this analysis are summarized in Table I [97].

Within the AMPT framework, the HIJING model generates hadrons, which are then transformed into their constituent quarks and antiquarks. The subsequent space-time evolution of these particles is determined using Zhang's parton cascade (ZPC) model [98], which incorporates the parton-scattering cross section:

$$\sigma_{pp} = \frac{9\pi\alpha_s^2}{2\mu^2}, \quad (4)$$

where α_s denotes the quantum chromodynamics (QCD) coupling constant and μ is the screening mass in the partonic matter; these parameters collectively shape the expansion dynamics of the collision systems [98]. Collisions were simulated for a fixed $\sigma_{pp} = 2.8$ [99,100]. Thus, the AMPT

model amalgamates several contributing factors: (i) the initial-state eccentricity, (ii) the initial parton-production stage governed by the HIJING model [101,102], (iii) a parton-scattering stage, (iv) the process of hadronization through coalescence, and finally, (v) a phase that encompasses interactions among the generated hadrons [103].

B. Analyses method

The multiparticle correlation technique with traditional and two-subevents cumulants methods [104–107] are used in this work. This study used the two subevents with a pseudorapidity gap $\Delta\eta = \eta_a - \eta_b > 0.7$ (i.e., $\eta_a > 0.35$ and $\eta_a < -0.35$) for the two-, three-, and four-particle correlations. However, I used the traditional cumulant method to calculate the five- and six-particle correlations. More details on the methods used can be found in Ref [16].

1. The k -particle symmetric correlations

The two-, four-, and six-particle symmetric correlations can be given using the multiparticle correlation techniques

$$\begin{aligned} SC(n_1, -n_1)|_{2\text{-Sub}} &= \langle\langle \cos(n_1\phi_{x1}^a - n_1\phi_{x2}^b) \rangle\rangle, \quad (5) \\ &= \langle\langle v_{n_1}^2 \cos(n_1\psi_{n_1} - n_1\psi_{n_1}) \rangle\rangle, \\ &= \langle\langle v_{n_1}^2 \rangle\rangle, \end{aligned}$$

where n_i is the harmonic order, ϕ_{x1}^a is the azimuthal angle of the particle x_1 in the subevent a , and the $\langle\langle \rangle\rangle$ defines the averaging first over particles in an event and then over events:

$$\begin{aligned} SC(n_1, n_2, -n_1, -n_2)_{2\text{-Sub}} &= \langle\langle \cos(n_1\phi_{x1}^a + n_2\phi_{x2}^a - n_1\phi_{x3}^b - n_2\phi_{x4}^b) \rangle\rangle, \\ &= \langle\langle v_{n_1}^2 v_{n_2}^2 \cos(n_1\psi_{n_1} + n_2\psi_{n_2} - n_1\psi_{n_1} - n_2\psi_{n_2}) \rangle\rangle, \\ &= \langle\langle v_{n_1}^2 v_{n_2}^2 \rangle\rangle, \quad (6) \end{aligned}$$

$$\begin{aligned} SC(n_1, n_2, n_3, -n_1, -n_2, -n_3)_{\text{Trad}} &= \langle\langle \cos(n_1\phi_{x1} + n_2\phi_{x2} + n_3\phi_{x3} - n_1\phi_{x4} - n_2\phi_{x5} - n_3\phi_{x6}) \rangle\rangle \\ &= \langle\langle v_{n_1}^2 v_{n_2}^2 v_{n_3}^2 \cos(n_1\psi_{n_1} + n_2\psi_{n_2} + n_3\psi_{n_3} - n_1\psi_{n_1} \\ &\quad - n_2\psi_{n_2} - n_3\psi_{n_3}) \rangle\rangle, \\ &= \langle\langle v_{n_1}^2 v_{n_2}^2 v_{n_3}^2 \rangle\rangle. \quad (7) \end{aligned}$$

2. The k -particle asymmetric correlations

The three-, four-, and five-particle asymmetric correlations can be given using the multiparticle correlation methods:

$$\begin{aligned} ASC(n_1, n_2, n_3)_{2\text{-Sub}} &= \langle\langle \cos(n_1\phi_{x1}^a + n_2\phi_{x2}^a + n_3\phi_{x3}^b) \rangle\rangle, \\ &= \langle\langle v_{n_1} v_{n_2} v_{n_3} \cos(n_1\psi_{n_1} + n_2\psi_{n_2} + n_3\psi_{n_3}) \rangle\rangle, \quad (8) \end{aligned}$$

$$\begin{aligned}
& ASC(n_1, n_2, n_3, n_4)_{2\text{-Sub}} \\
&= \langle\langle \cos(n_1\phi_{x1}^a + n_2\phi_{x2}^a + n_3\phi_{x3}^b + n_4\phi_{x4}^b) \rangle\rangle, \\
&= \langle\langle v_{n_1}v_{n_2}v_{n_3}v_{n_4} \cos(n_1\psi_{n_1} + n_2\psi_{n_2} + n_3\psi_{n_3} + n_4\psi_{n_4}) \rangle\rangle, \tag{9}
\end{aligned}$$

$$\begin{aligned}
& ASC(n_1, n_2, n_3, n_4, n_5)_{\text{Trad}} \\
&= \langle\langle \cos(n_1\phi_{x1} + n_2\phi_{x2} + n_3\phi_{x3} + n_4\phi_{x4} + n_5\phi_{x5}) \rangle\rangle, \\
&= \langle\langle v_{n_1}v_{n_2}v_{n_3}v_{n_4}v_{n_5} \cos(n_1\psi_{n_1} + n_2\psi_{n_2} + n_3\psi_{n_3} + n_4\psi_{n_4} \\
&\quad + n_5\psi_{n_5}) \rangle\rangle. \tag{10}
\end{aligned}$$

3. The k -particle normalized symmetric correlations

The multiparticle correlations Eqs. (5) and (6) can be used to give the same and mix order flow harmonics NSC as [31,35]

$$\gamma_{n_1, n_1, -n_1, -n_1} = 2 - \frac{SC(n_1, n_1, -n_1, -n_1)_{2\text{-Sub}}}{SC(n_1, -n_1)_{2\text{-Sub}}SC(n_1, -n_1)_{2\text{-Sub}}}, \tag{11}$$

4. The k -particle normalized asymmetric correlations

The multiparticle correlations Eqs. (5)–(7) can define the normalized asymmetric correlations, which gives the flow angle (ψ_n) correlations as [35,87,112]

$$\begin{aligned}
\rho_{n_1, n_2, n_3} &= \frac{ASC(n_1, n_2, n_3)_{2\text{-Sub}}}{\sqrt{|SC(n_1, n_2, -n_1, -n_2)_{2\text{-Sub}}SC(n_3, -n_3)_{2\text{-Sub}}|}} \\
&\sim \langle\langle \cos(n_1\psi_{n_1} + n_2\psi_{n_2} + n_3\psi_{n_3}) \rangle\rangle. \tag{13}
\end{aligned}$$

$$\begin{aligned}
\rho_{n_1, n_2, n_3, n_4} &= \frac{ASC(n_1, n_2, n_3, n_4)_{2\text{-Sub}}}{\sqrt{|SC(n_1, n_2, n_3, -n_1, -n_2, -n_3)_{\text{Trad}}SC(n_4, -n_4)_{2\text{-Sub}}|}} \\
&\sim \langle\langle \cos(n_1\psi_{n_1} + n_2\psi_{n_2} + n_3\psi_{n_3} + n_4\psi_{n_4}) \rangle\rangle. \tag{14}
\end{aligned}$$

$$\begin{aligned}
\rho_{n_1, n_2, n_3, n_4, n_5} &= \frac{ASC(n_1, n_2, n_3, n_4, n_5)_{\text{Trad}}}{\sqrt{|SC(n_1, n_2, n_3, -n_1, -n_2, -n_3)_{\text{Trad}}SC(n_4, n_5, -n_4, -n_5)_{2\text{-Sub}}|}} \\
&\sim \langle\langle \cos(n_1\psi_{n_1} + n_2\psi_{n_2} + n_3\psi_{n_3} + n_4\psi_{n_4} + n_5\psi_{n_5}) \rangle\rangle. \tag{15}
\end{aligned}$$

The definitions given in Eqs. (13), (14), and (15) are in line with the definition used by the ALICE and STAR experiments [87,112].

III. RESULTS AND DISCUSSION

This section will discuss the prediction of the k -particle symmetric (asymmetric) correlations and the flow harmonics magnitude and angular correlations in the isobaric collisions for different initial state configurations given in Table I. Here, it is important to note that the nonflow effects on the presented results have been investigated in my previous study Ref. [16].

A. Symmetric correlations

Figures 1–3 show the centrality and system size dependencies of the two-, four-, and six-particle symmetric correlations. The comparisons of the same flow harmonic two-, four-, and six-particle correlations are expected to reflect the initial state density fluctuations and the final state hydrodynamic

$$\beta_{n_1, n_2, -n_1, -n_2} = \frac{SC(n_1, n_2, -n_1, -n_2)_{2\text{-Sub}}}{SC(n_1, -n_1)_{2\text{-Sub}}SC(n_2, -n_2)_{2\text{-Sub}}} - 1. \tag{12}$$

Note that Eq. (11) can also be written as $-C_n\{4\}/C_n\{2\}$, where $C_n\{2\}$ and $C_n\{4\}$ are the second- and fourth-order cumulant of the v_n distribution [104,105,108–110].

The ratio $\gamma_{n,n,-n,-n}$ is a metric for the n th harmonic flow fluctuations. In the absence of event-by-event fluctuations, $\gamma_{n,n,-n,-n} = 1$ for the Bessel-Gaussian distribution of the v_2 , while $0 < \gamma_{n,n,-n,-n} < 1$ quantifies the strength of the flow fluctuations [111]. For $n = 3$, $\gamma_{n,n,-n,-n} = 0$ the v_3 has a Gaussian distribution, while $\gamma_{n,n,-n,-n} \neq 0$ quantifies the deviation from Gaussianity. The ratio $\beta_{n,m,-n,-m}$ estimates the mixed harmonics flow correlations: (i) $\beta_{n,m,-n,-m} = 0.0$ represents the absence of the flow correlations, (ii) $\beta_{n,m,-n,-m} > 0.0$ denotes the mode-coupling strength between the n and m flow harmonics, and (iii) $\beta_{n,m,-n,-m} < 0.0$ gives the strength of anticorrelation between the n and m harmonics.

evolution fluctuations [42]. The same harmonic correlations ($n > 1$) from the AMPT model at the same σ_{pp} present characteristic patterns from central to peripheral collisions (i.e., increasing from central to midcentral collisions, then decreasing as the collisions become more peripheral). Such characteristic patterns display the interplay between initial-state eccentricities and final-state viscous attenuation [113]. Note that the $n = 1$ correlations will be impacted by the global momentum conservation (GMC) effect [47,114], which have been recently studied in the isobaric collisions [56].

The four- and six-particle mixed harmonics correlations as a function of centrality for Ru + Ru and Zr + Zr at $\sqrt{s_{NN}} = 200$ GeV from the AMPT model with various parameters given in Table I are presented in Figs. 4–7. These mixed harmonics flow correlations are expected to give the flow harmonics magnitude correlations induced by initial and final state effects, which will be provided employing the ratios defined in Eq. (12). The correlations presented in Figs. 4–7 are sensitive to the interplay between final and initial state effects

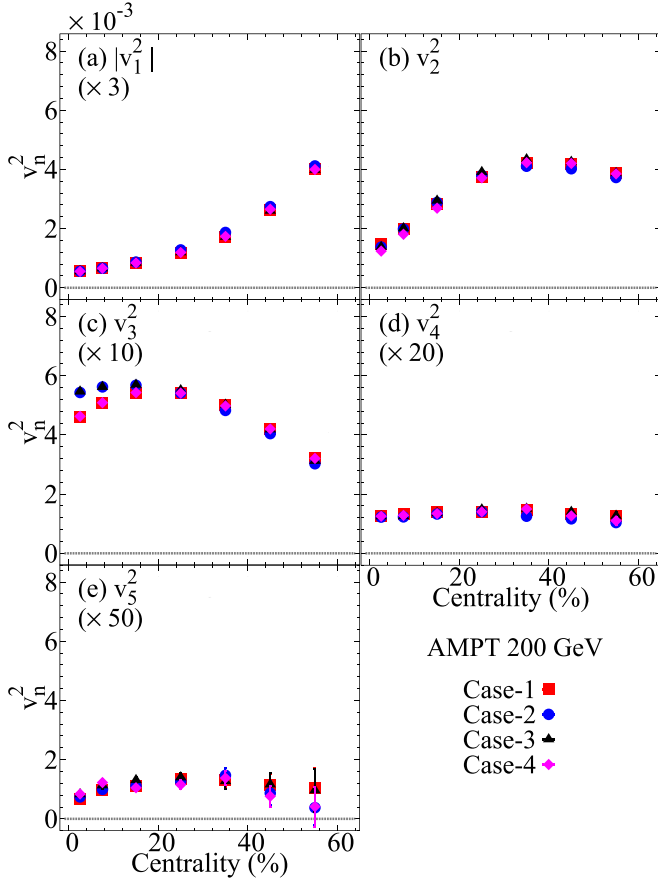


FIG. 1. Comparisons of the centrality dependence of the two-particle flow harmonics $v_n^2 = SC(n, -n)$ using the two-subevents method for Ru + Ru and Zr + Zr at $\sqrt{s_{NN}} = 200$ GeV from the AMPT model with various parameters given in Table I.

[16]. The mixed harmonics correlations with $n = 1$, Fig. 4, are expected to be impacted by the GMC effect.

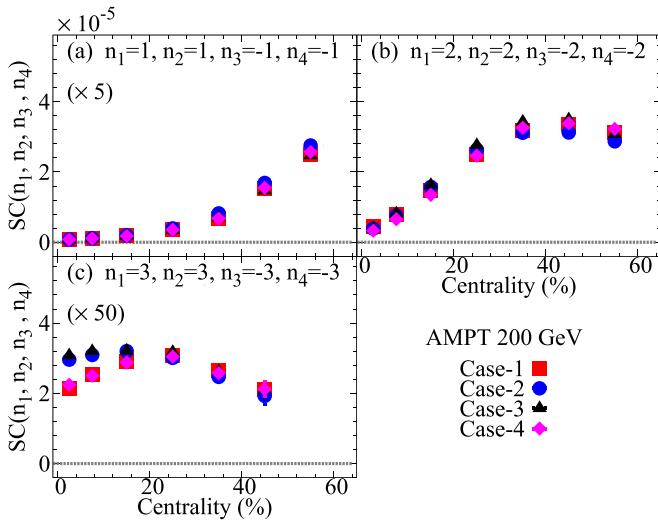


FIG. 2. Same as in Fig. 1 but for the four-particle $SC(1, 1, -1, -1)$ (a), $SC(2, 2, -2, -2)$ (b), and $SC(3, 3, -3, -3)$ (c) using the two-subevents method.

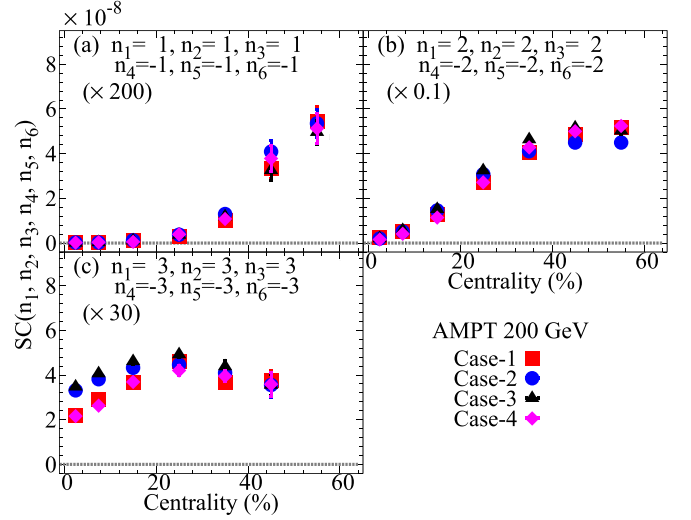


FIG. 3. Same as in Fig. 1 but for the six-particle $SC(1, 1, 1, -1, -1, -2)$ (a), $SC(2, 2, 2, -2, -2, -2)$ (b), and $SC(3, 3, 3, -3, -3, -3)$ (c), using the one-subevent method.

B. Asymmetric correlations

Using the symmetric and asymmetric correlations, I can get the flow angular correlations induced by the initial state and given by Eqs. (13)–(15). Therefore, it is constructive first to discuss the centrality and system size dependence of asymmetric correlations.

The three-, four-, and five-particle asymmetric correlations for Ru + Ru and Zr + Zr at $\sqrt{s_{NN}} = 200$ GeV from the AMPT model are shown in Figs. 8–11. The presented AMPT calculations of the ASC Figs. 8–11 show that the strength of the correlation gets stronger as the collisions become more peripheral. In contrast, the $ASC(2, 2, 2, -3, -3)$ values in Fig. 11(b) are consistent with zero, reflecting the weak correlation nature between ψ_2 and ψ_3 .

C. Normalized symmetric correlations

In the previous studies [16,25], I pointed out that the flow harmonics magnitude fluctuations and correlations have a weak sensitivity to the final state effects. Therefore, they can constrain the HIC initial conditions [42,112]. The flow harmonics magnitude fluctuations and correlations can be given

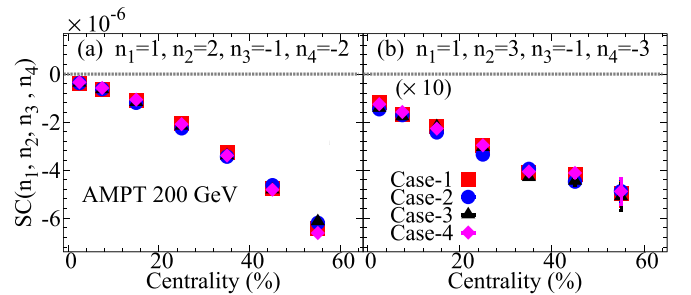


FIG. 4. Same as in Fig. 1 but for the four-particle $SC(1, 2, -1, -2)$ (a) and $SC(1, 3, -1, -3)$ (b), using the two-subevent method.

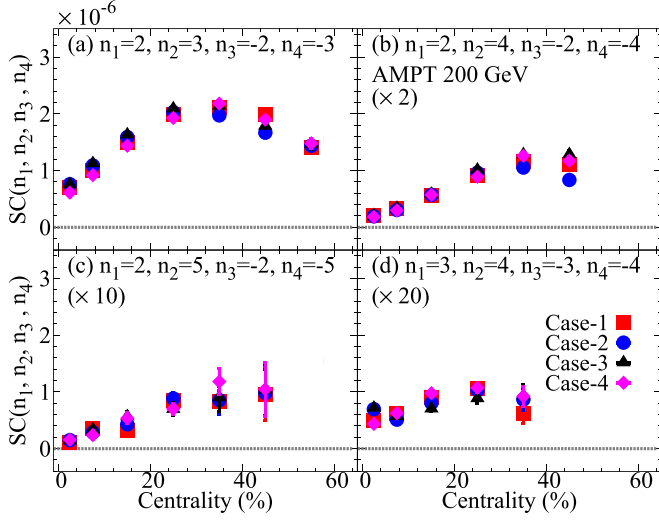


FIG. 5. Same as in Fig. 1 but for the four-particle $SC(2, 3, -2, -3)$ (a), $SC(2, 4, -2, -4)$ (b), $SC(2, 4, -2, -4)$ (c), and $SC(3, 4, -3, -4)$ (d), using the two-subevent method.

$\gamma_{n,n,-n,-n}$ Eq. (11) and $\beta_{n,m,-n,-m}$ Eq. (12), respectively. For NSC, I will present the AMPT model calculations for Case-1 and Case-2 parameters see Table I.

The normalized symmetric correlations for the same flow harmonic, $\gamma_{1,1,-1,-1}$, $\gamma_{2,2,-2,-2}$ and $\gamma_{3,3,-3,-3}$ are presented in Fig. 12 for Ru + Ru and Zr + Zr at $\sqrt{s_{NN}} = 200$ GeV from the AMPT model Case-1 and Case-2. In panel (a), the $\gamma_{1,1,-1,-1}$ indicates the rapidity-even dipolar flow fluctuations in the AMPT model. The $\gamma_{1,1,-1,-1}$ calculations assume equivalent GMC effects on the $n = 1$ two- and four-particle correlations. These calculations indicated an apparent difference in the fluctuation nature between the $\gamma_{1,1,-1,-1}$ calculated for initial and final states in the AMPT model. The elliptic flow fluctuations are given in panel (b) by the $\gamma_{2,2,-2,-2}$; it

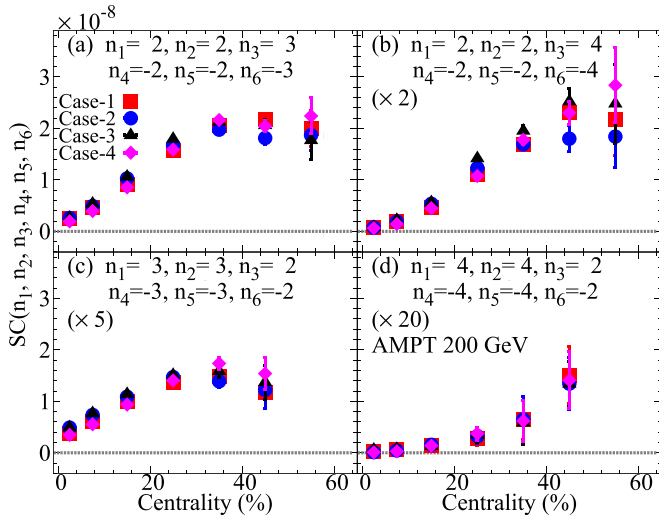


FIG. 6. Same as in Fig. 1 but for the six-particle symmetric correlations $SC(2, 2, 3, -2, -2, -3)$ (a), $SC(2, 2, 4, -2, -2, -4)$ (b), $SC(3, 3, 2, -3, -3, -2)$ (c), and $SC(4, 4, 2, -4, -4, -2)$ (d), using the one-subevent method.

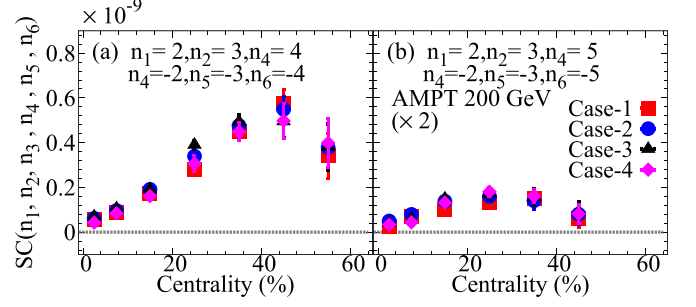


FIG. 7. Same as in Fig. 1 but for the six-particle symmetric correlations $SC(2, 3, 4, -2, -3, -4)$ (a) and $SC(2, 3, 5, -2, -3, -5)$ (b), using the one-subevent method.

indicates the anticipated reduction in the fluctuations magnitude from central to peripheral collisions. I observe an agreement between $\gamma_{2,2,-2,-2}$ calculated for initial and final states in the AMPT model in central collisions. In contrast, I observed less fluctuations in the initial state $\gamma_{2,2,-2,-2}$. The latter observation suggests that the AMPT final state effects add more fluctuations to the elliptic flow. The ratio $\gamma_{3,3,-3,-3}$ in panel (c) presents the triangular flow fluctuations. The $\gamma_{3,3,-3,-3}$ from the AMPT model is consistent with zero with significant uncertainties for both systems, which is consistent with the STAR measurements [115] and the prior AMPT calculations [16] for Au+Au at 200 GeV.

Figure 13 show the mixed flow harmonics NSC $\beta_{1,2,-1,-2}$ (a), $\beta_{1,3,-1,-3}$ (b), $\beta_{2,3,-2,-3}$ (c), and $\beta_{2,4,-2,-4}$ (d) for Ru + Ru and Zr + Zr at $\sqrt{s_{NN}} = 200$ GeV from the AMPT model Case-1 and Case-2. The correlations between the rapidity-even dipolar flow v_1 and the v_2 and v_3 magnitudes given in panels (a) and (b) suppose equal GMC effects on the $n = 1$ two- and four-particle correlations. The $\beta_{1,2,-1,-2}$ and $\beta_{1,3,-1,-3}$ initial and final state calculations indicated

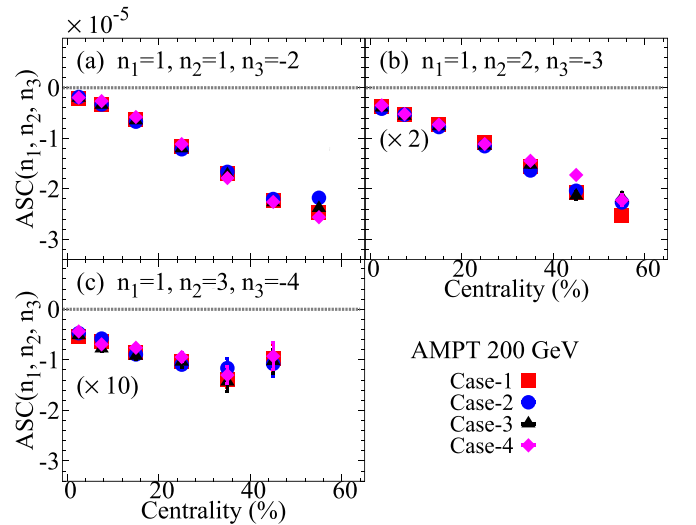


FIG. 8. Comparisons of the centrality dependence of the three-particle asymmetric correlations $ASC(1, 1, -2)$ (a), $ASC(1, 2, -3)$ (b), and $ASC(1, 3, -4)$ (c), using the two-subevents method for Ru + Ru and Zr + Zr at $\sqrt{s_{NN}} = 200$ GeV from the AMPT model with various parameters given in Table I.

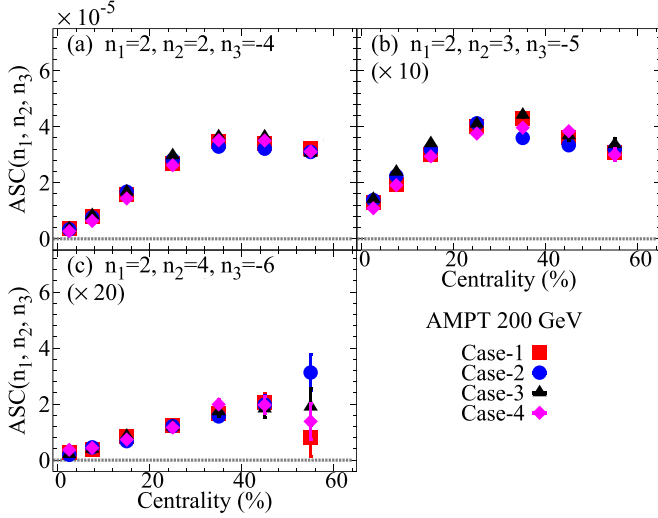


FIG. 9. Same as in Fig. 8 but for the three-particle asymmetric correlations $ASC(2, 2, -4)$ (a), $ASC(2, 3, -5)$ (b), and $ASC(2, 4, -5)$ (c), using two-subevents method.

anticorrelations between v_1 and v_n ($n = 2, 3$). On the other hand, the v_2 - v_n ($n = 3$ and 4) correlations nature are given by $\beta_{2,3,-2,-3}$, $\beta_{2,4,-2,-4}$ in panels (c) and (d). The initial and final state calculations show anticorrelations between v_2 and v_3 , with larger strength for the initial state calculations. In contrast, I observed positive correlations between v_2 and v_4 from initial and final state results, with much smaller strength for the initial state calculations.

D. Normalized asymmetric correlations

An additional understanding of the HIC initial conditions [112] can be gained by studying the flow angular correlations via the normalized asymmetric correlations Eqs. (13)–(15). The NASC ρ_X is expected to operate as a metric for the

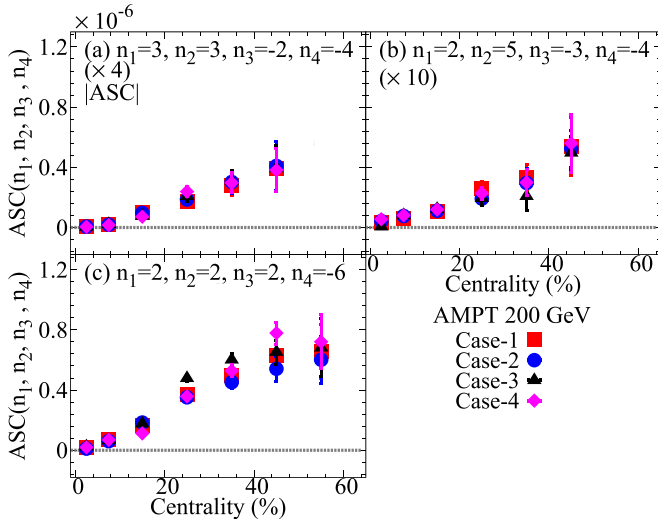


FIG. 10. Same as in Fig. 8 but for the four-particle asymmetric correlations $ASC(3, 3, -2, -4)$ (a), $ASC(2, 5, -3, -4)$ (b), and $ASC(2, 2, 2, -6)$ (c), using two-subevents method.

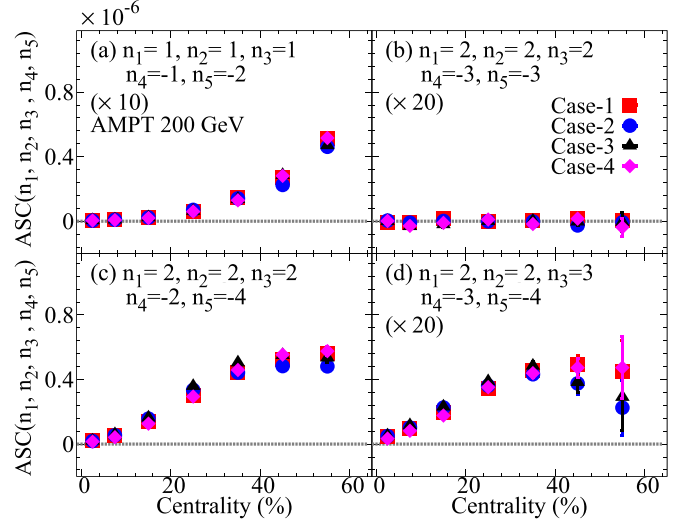


FIG. 11. Same as in Fig. 8 but for the five-particle asymmetric correlations $ASC(1, 1, 1, -1, -2)$ (a), $ASC(2, 2, 2, -3, -3)$ (b), $ASC(2, 2, 2, -2, -4)$ (c), and $ASC(2, 2, 3, -3, -4)$ (d), using one-subevent method.

strength of the correlations between flow symmetry planes (i.e., ψ_1 - ψ_5) see Table II.

Figure 14 shows the centrality and the system size dependence of the event planes' angular correlations $\langle \cos(2\psi_1 - 2\psi_2) \rangle$ (a), $\langle \cos(6\psi_2 - 6\psi_3) \rangle$ (b), $\langle \cos(4\psi_2 - 4\psi_4) \rangle$ (c), and $\langle \cos(6\psi_2 - 6\psi_6) \rangle$ (d) for Ru + Ru and Zr + Zr at $\sqrt{s_{NN}} = 200$ GeV from the AMPT model Case-1 and Case-2 parameters given in Table I. The ratios $\rho_{1,1,-2}$ and $\rho_{1,1,1,-1,-2}$ are in agreement and increase with centrality selections. The observed agreement between $\rho_{1,1,-2}$ and $\rho_{1,1,1,-1,-2}$ suggest that $\rho_{1,1,-2}$ and $\rho_{1,1,1,-1,-2}$ have a similar contribution from the GMC effects. In addition, I found a good agreement in

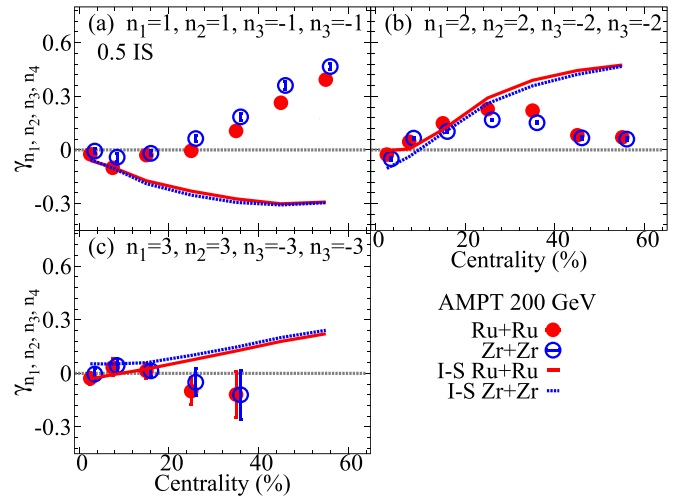


FIG. 12. Comparisons of the centrality dependence of the same harmonic normalized symmetric correlations $\gamma_{1,1,-1,-1}$ (a), $\gamma_{2,2,-2,-2}$ (b), and $\gamma_{3,3,-3,-3}$ (c), for Ru + Ru and Zr + Zr at $\sqrt{s_{NN}} = 200$ GeV from the AMPT model Case-1 and Case-2 parameters given in Table I. The curves represent the initial state eccentricity fluctuations.

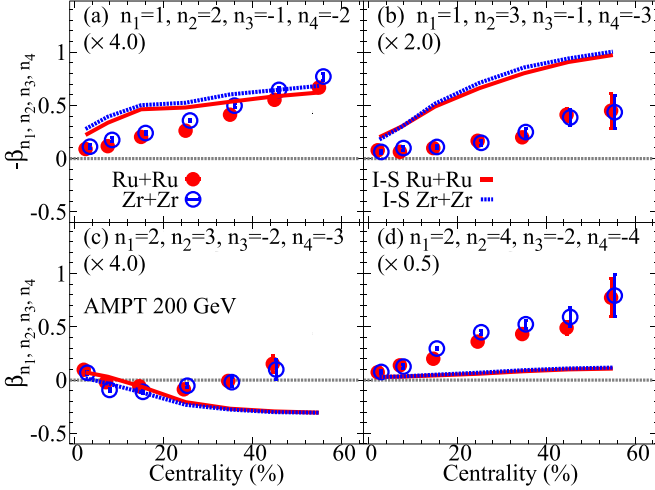


FIG. 13. Same as in Fig. 12 but for the mixed harmonic normalized symmetric correlations $\beta_{1,2,-1,-2}$ (a), $\beta_{1,3,-1,-3}$ (b), $\beta_{2,3,-2,-3}$ (c), $\beta_{2,4,-2,-4}$ (d), $\beta_{2,5,-2,-5}$ (e), and $\beta_{3,4,-3,-4}$ (f).

central collisions between the initial and final state constructed $\langle \cos(2\psi_1 - 2\psi_2) \rangle$. In panel (b), I demonstrated the expected absence of correlations between ψ_2 and ψ_3 by presenting the vanishing values of the $\rho_{2,2,2,-3,-3}$ ratios. The present results agree with the expectation that ψ_3 is a fluctuation-driven event plane. The ratios $\rho_{2,2,-4}$, $\rho_{2,2,2,-2,-4}$, and $\rho_{2,2,3,-3,-4}$ panel (c) give the correlation between ψ_2 and ψ_4 ($\langle \cos(4\psi_2 - 4\psi_4) \rangle$), the results show a reasonable agreement between the three ratios. Also, I presented the positive correlations between ψ_2 and ψ_6 ($\langle \cos(6\psi_2 - 6\psi_6) \rangle$) given by the ratio $\rho_{2,4,-6}$. The present calculations indicated a disagreement in values between the ρ_X estimated from initial and final state for $\psi_2-\psi_4$ and $\psi_2-\psi_6$ correlations.

The system size and centrality dependence of the NASC $\rho_{1,2,-3}$, $\rho_{1,3,-4}$, $\rho_{2,3,-5}$, and $\rho_{3,3,-2,-4}$ are shown in Fig. 15. The three event planes correlations $\langle \cos(1\psi_1 + 2\psi_2 - 3\psi_3) \rangle$, $\langle \cos(1\psi_1 + 3\psi_2 - 4\psi_4) \rangle$, $\langle \cos(2\psi_2 + 3\psi_3 - 5\psi_5) \rangle$, and $\langle \cos(6\psi_3 - 2\psi_2 - 4\psi_4) \rangle$ indicated an increase with centrality selections for both initial and final state correlators. The present results showed a negative correlation for

TABLE II. The summary of the NASC that is presented in this work.

Event-plane angular correlations	NASC
$\langle \cos(2\psi_1 - 2\psi_2) \rangle$	$\rho_{1,1,-2}$
$\langle \cos(6\psi_2 - 6\psi_3) \rangle$	$\rho_{1,1,1,-1,-2}$
$\langle \cos(4\psi_2 - 4\psi_4) \rangle$	$\rho_{2,2,2,-3,-3}$
$\langle \cos(6\psi_2 - 6\psi_6) \rangle$	$\rho_{2,2,-4}$
$\langle \cos(1\psi_1 + 2\psi_2 - 3\psi_3) \rangle$	$\rho_{2,2,2,-2,-4}$
$\langle \cos(1\psi_1 + 3\psi_2 - 4\psi_4) \rangle$	$\rho_{2,2,3,-3,-4}$
$\langle \cos(2\psi_2 + 3\psi_3 - 5\psi_5) \rangle$	$\rho_{2,2,2,-6}$
$\langle \cos(6\psi_3 - 2\psi_2 - 4\psi_4) \rangle$	$\rho_{1,2,-3}$
	$\rho_{1,3,-4}$
	$\rho_{2,3,-5}$
	$\rho_{3,3,-2,-4}$

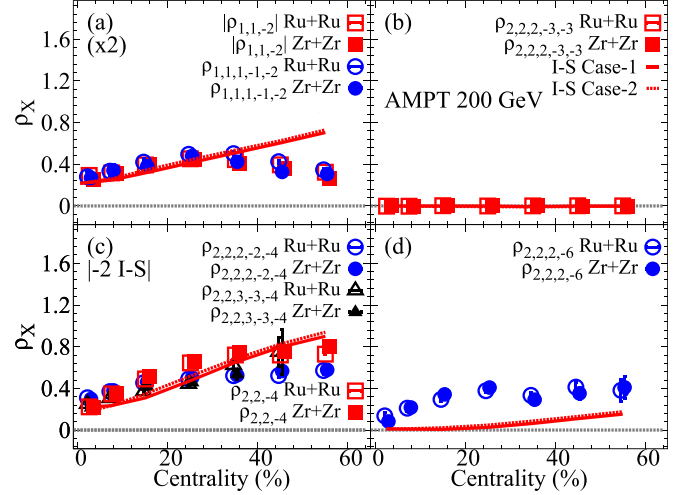


FIG. 14. Comparisons of the centrality dependence of the normalized asymmetric correlations $\rho_{1,1,-2}$ and $\rho_{1,1,1,-1,-2}$ (a), $\rho_{2,2,2,-3,-3}$ (b), $\rho_{2,2,-4}$, $\rho_{2,2,2,-2,-4}$, and $\rho_{2,2,3,-3,-4}$ (c), and $\rho_{2,4,-6}$ (d), for Ru + Ru and Zr + Zr at $\sqrt{s_{NN}} = 200$ GeV from the AMPT model Case-1 and Case-2 parameters given in Table I. The curves represent the initial state eccentricity fluctuations.

$\langle \cos(6\psi_3 - 2\psi_2 - 4\psi_4) \rangle$ that disagree with the initial state estimate. The present AMPT calculations for both isobars indicated a disagreement in magnitude between the initial and final state calculations.

E. Sensitivity to the deformations and nuclear skin

Many prior investigations into anisotropic flow observables, especially the ratios involving Ru + Ru and Zr + Zr, have underscored the sensitivity of these observables to nuclear deformations and skin [[53,55,56,60,61,64,70,71,74,116–119]. These studies have highlighted that, in central collisions, the lower-order flow harmonics ($n < 4$) exhibit sensitivity to the β_2 and β_3 . Higher-order flow harmonics are expected to be sensitive to

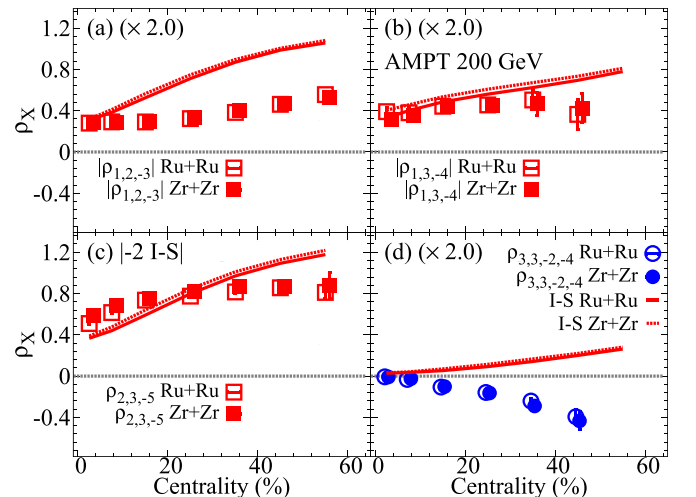


FIG. 15. Same as in Fig. 14 but for $\rho_{1,2,-3}$ (a), $\rho_{1,3,-4}$ (b), $\rho_{2,3,-5}$, $\rho_{2,3,2,-2,-5}$, and $\rho_{2,3,3,-3,-5}$ (c), and $\rho_{3,3,-2,-4}$ and $\rho_{2,3,3,-4,-4}$ (d).

the interplay between lower- and higher-order deformation parameters. Also, it has been noted that at noncentral collisions, the anisotropic flow observables are more susceptible to the change in the nuclear skin.

In this study, my focus is on the absolute values of the observables rather than the Ru + Ru and Zr + Zr ratios. At the absolute values level, the present SC results, illustrated in Figs. 1–3, indicate sensitivity to nuclear deformation in central collisions and nuclear skin in noncentral collisions. Figures. 4–11 present the mixed harmonics (A)SC, expected to be sensitive to the interplay between lower- and higher-order deformation parameters in central collisions. Additionally, the NSC and NASC Figs. 12–15, anticipated to be sensitive to initial-state effects, demonstrate sensitivity to nuclear deformation and skin in central and noncentral collisions, respectively. These observations suggest that the presented observables have the potential to constrain the differences in nuclear deformation and skin between ^{96}Ru and ^{96}Zr .

IV. SUMMARY AND OUTLOOK

This study utilizes the AMPT model to predict symmetric correlations (SC), asymmetric correlations (ASC), normalized symmetric correlations (NSC), and normalized asymmetric correlations (NASC) for Ru + Ru and Zr + Zr at RHIC top energy. The presented calculations can be categorized as follows:

- (i) Symmetric and asymmetric correlations: The SC and ASC, as depicted in Figs. 1–11, are anticipated to

be sensitive to the interplay between initial and final state effects. Thus, the SC and ASC can validate the assumption that isobaric ratios effectively cancel the final state effect between the two isobars. Moreover, they can constrain the interplay between initial and final state effects in theoretical calculations.

- (ii) Normalized symmetric and asymmetric correlations: The NSC and NASC, shown in Figs. 12–15, are predicted to be primarily influenced by initial state effects. Consequently, the NSC and NASC are better suited for studying nuclear structure differences between ^{96}Ru and ^{96}Zr . The present results for Ru + Ru and Zr + Zr reveal a noticeable discrepancy between initial and final state calculations, emphasizing the necessity for a data-model comparison.

In summary, this work presents the centrality dependence of SC, ASC, NSC, and NASC from the AMPT model for Ru + Ru and Zr + Zr at 200 GeV. This study offers a detailed prediction of these correlations for Ru + Ru and Zr + Zr collisions at RHIC top energy, considering differences in geometry and structure between ^{96}Ru and ^{96}Zr . I conclude that conducting detailed comparisons between future experimental measurements and the present calculations will aid in constraining the initial and final state effects of the AMPT model.

ACKNOWLEDGMENTS

The author thanks S. Bhatta and Dr. E. Racow for the valuable discussions and for pointing out essential references.

-
- [1] P. Danielewicz, R. A. Lacey, P. B. Gossiaux, C. Pinkenburg, P. Chung, J. M. Alexander, and R. L. McGrath, *Phys. Rev. Lett.* **81**, 2438 (1998).
 - [2] K. Ackermann *et al.* (STAR Collaboration), *Phys. Rev. Lett.* **86**, 402 (2001).
 - [3] K. Adcox *et al.* (PHENIX Collaboration), *Phys. Rev. Lett.* **89**, 212301 (2002).
 - [4] U. W. Heinz and P. F. Kolb, Statistical QCD, Proceedings of the International Symposium, Bielefeld, Germany, August 26–30, 2001 [*Nucl. Phys. A* **702**, 269 (2002)].
 - [5] T. Hirano, U. W. Heinz, D. Kharzeev, R. Lacey, and Y. Nara, *Phys. Lett. B* **636**, 299 (2006).
 - [6] P. Huovinen, P. F. Kolb, U. W. Heinz, P. V. Ruuskanen, and S. A. Voloshin, *Phys. Lett. B* **503**, 58 (2001).
 - [7] T. Hirano and K. Tsuda, *Phys. Rev. C* **66**, 054905 (2002).
 - [8] P. Romatschke and U. Romatschke, *Phys. Rev. Lett.* **99**, 172301 (2007).
 - [9] M. Luzum, *J. Phys. G* **38**, 124026 (2011).
 - [10] H. Song, S. A. Bass, U. Heinz, T. Hirano, and C. Shen, *Phys. Rev. Lett.* **106**, 192301 (2011); **109**, 139904(E) (2012).
 - [11] J. Qian, U. W. Heinz, and J. Liu, *Phys. Rev. C* **93**, 064901 (2016).
 - [12] B. Schenke, S. Jeon, and C. Gale, *Phys. Lett. B* **702**, 59 (2011).
 - [13] D. Teaney and L. Yan, *Phys. Rev. C* **86**, 044908 (2012).
 - [14] F. G. Gardim, F. Grassi, M. Luzum, and J.-Y. Ollitrault, *Phys. Rev. Lett.* **109**, 202302 (2012).
 - [15] R. A. Lacey, D. Reynolds, A. Taranenko, N. N. Ajitanand, J. M. Alexander, F.-H. Liu, Y. Gu, and A. Mwai, *J. Phys. G* **43**, 10LT01 (2016).
 - [16] N. Magdy, *Phys. Rev. C* **107**, 024905 (2023).
 - [17] D. Teaney, *Phys. Rev. C* **68**, 034913 (2003).
 - [18] R. A. Lacey and A. Taranenko, Correlations and fluctuations in relativistic nuclear collisions. Proceedings, 2nd International Workshop, CFRNC2006, Florence, Italy, July 7–9, 2006, *PoS CFRNC2006*, 021 (2007).
 - [19] H. Song, S. A. Bass, and U. Heinz, *Phys. Rev. C* **83**, 054912 (2011).
 - [20] B. Alver and G. Roland, *Phys. Rev. C* **81**, 054905 (2010); **82**, 039903(E) (2010).
 - [21] B. Schenke, S. Jeon, and C. Gale, *Phys. Rev. Lett.* **106**, 042301 (2011).
 - [22] C. Shen, U. Heinz, P. Huovinen, and H. Song, *Phys. Rev. C* **82**, 054904 (2010).
 - [23] H. Niemi, G. S. Denicol, P. Huovinen, E. Molnar, and D. H. Rischke, *Phys. Rev. C* **86**, 014909 (2012).
 - [24] G.-Y. Qin, H. Petersen, S. A. Bass, and B. Muller, *Phys. Rev. C* **82**, 064903 (2010).
 - [25] N. Magdy, *Universe* **9**, 107 (2023).

- [26] S. Voloshin and Y. Zhang, *Z. Phys. C* **70**, 665 (1996).
- [27] A. M. Poskanzer and S. A. Voloshin, *Phys. Rev. C* **58**, 1671 (1998).
- [28] F. G. Gardim, F. Grassi, M. Luzum, and J.-Y. Ollitrault, *Phys. Rev. C* **85**, 024908 (2012).
- [29] H. Niemi, G. S. Denicol, H. Holopainen, and P. Huovinen, *Phys. Rev. C* **87**, 054901 (2013).
- [30] J. Adam *et al.* (STAR Collaboration), *Phys. Lett. B* **783**, 459 (2018).
- [31] J. Adam *et al.* (ALICE Collaboration), *Phys. Rev. Lett.* **117**, 182301 (2016).
- [32] L. Adamczyk *et al.* (STAR Collaboration), *Phys. Rev. C* **98**, 034918 (2018).
- [33] Z. Qiu and U. W. Heinz, *Phys. Rev. C* **84**, 024911 (2011).
- [34] A. Adare *et al.* (PHENIX Collaboration), *Phys. Rev. Lett.* **107**, 252301 (2011).
- [35] G. Aad *et al.* (ATLAS Collaboration), *Phys. Rev. C* **90**, 024905 (2014).
- [36] G. Aad *et al.* (ATLAS Collaboration), *Phys. Rev. C* **92**, 034903 (2015).
- [37] N. Magdy (STAR Collaboration), Proceedings of the 27th International Conference on Ultrarelativistic Nucleus-Nucleus Collisions (Quark Matter 2018), Venice, Italy, May 14–19, 2018 [*Nucl. Phys. A* **982**, 255 (2019)].
- [38] B. Alver *et al.* (PHOBOS Collaboration), *Phys. Rev. C* **77**, 014906 (2008).
- [39] B. Alver *et al.* (PHOBOS Collaboration), *Phys. Rev. C* **81**, 034915 (2010).
- [40] J.-Y. Ollitrault, A. M. Poskanzer, and S. A. Voloshin, *Phys. Rev. C* **80**, 014904 (2009).
- [41] N. Magdy, *Phys. Rev. C* **106**, 044911 (2022).
- [42] M. Abdallah *et al.* (STAR Collaboration), *Phys. Rev. Lett.* **129**, 252301 (2022).
- [43] L. Adamczyk *et al.* (STAR Collaboration), *Phys. Rev. C* **94**, 034908 (2016).
- [44] L. Adamczyk *et al.* (STAR Collaboration), *Phys. Rev. C* **93**, 014907 (2016).
- [45] L. Adamczyk *et al.* (STAR Collaboration), *Phys. Rev. Lett.* **115**, 222301 (2015).
- [46] L. Adamczyk *et al.* (STAR Collaboration), *Phys. Rev. Lett.* **116**, 112302 (2016).
- [47] J. Adam *et al.* (STAR Collaboration), *Phys. Rev. Lett.* **122**, 172301 (2019).
- [48] F. G. Gardim, J. Noronha-Hostler, M. Luzum, and F. Grassi, *Phys. Rev. C* **91**, 034902 (2015).
- [49] J. Fu, *Phys. Rev. C* **92**, 024904 (2015).
- [50] H. Holopainen, H. Niemi, and K. J. Eskola, *Phys. Rev. C* **83**, 034901 (2011).
- [51] C. Gale, S. Jeon, B. Schenke, P. Tribedy, and R. Venugopalan, *Phys. Rev. Lett.* **110**, 012302 (2013).
- [52] P. Liu and R. A. Lacey, *Phys. Rev. C* **98**, 021902(R) (2018).
- [53] J. Jia, *Phys. Rev. C* **105**, 014905 (2022).
- [54] G. Giacalone, J. Jia, and C. Zhang, *Phys. Rev. Lett.* **127**, 242301 (2021).
- [55] N. Magdy, *Eur. Phys. J. A* **59**, 64 (2023).
- [56] N. Magdy and R. Lacey, [arXiv:2308.11031](https://arxiv.org/abs/2308.11031).
- [57] P. Filip, *Phys. At. Nucl.* **71**, 1609 (2008).
- [58] J. Jia, S. Huang, and C. Zhang, *Phys. Rev. C* **105**, 014906 (2022).
- [59] H. Li, H. J. Xu, J. Zhao, Z.-W. Lin, H. Zhang, X. Wang, C. Shen, and F. Wang, *Phys. Rev. C* **98**, 054907 (2018).
- [60] H. Li, H. J. Xu, Y. Zhou, X. Wang, J. Zhao, L.-W. Chen, and F. Wang, *Phys. Rev. Lett.* **125**, 222301 (2020).
- [61] H.-J. Xu, H. Li, X. Wang, C. Shen, and F. Wang, *Phys. Lett. B* **819**, 136453 (2021).
- [62] H. J. Xu, H. Li, Y. Zhou, X. Wang, J. Zhao, L.-W. Chen, and F. Wang, *Phys. Rev. C* **105**, L011901 (2022).
- [63] H. J. Xu, W. Zhao, H. Li, Y. Zhou, L.-W. Chen, and F. Wang, *Phys. Rev. C* **108**, L011902 (2023).
- [64] S. Zhao, H.-J. Xu, Y.-X. Liu, and H. Song, *Phys. Lett. B* **839**, 137838 (2023).
- [65] H. Xu (STAR Collaboration), *Acta Phys. Pol. Supp.* **16**, 30 (2023).
- [66] J.-F. Wang, H.-J. Xu, and F. Wang, [arXiv:2305.17114](https://arxiv.org/abs/2305.17114).
- [67] A. Dimri, S. Bhatta, and J. Jia, *Eur. Phys. J. A* **59**, 45 (2023).
- [68] L.-M. Liu, C.-J. Zhang, J. Xu, J. Jia, and G.-X. Peng, *Phys. Rev. C* **106**, 034913 (2022).
- [69] M. Nie, C. Zhang, Z. Chen, L. Yi, and J. Jia, *Phys. Lett. B* **845**, 138177 (2023).
- [70] J. Jia, G. Giacalone, and C. Zhang, *Phys. Rev. Lett.* **131**, 022301 (2023).
- [71] J. Jia, G. Giacalone, and C. Zhang, *Chin. Phys. Lett.* **40**, 042501 (2023).
- [72] C. Zhang, S. Bhatta, and J. Jia, *Phys. Rev. C* **106**, L031901 (2022).
- [73] J. Jia, G. Wang, and C. Zhang, *Phys. Lett. B* **833**, 137312 (2022).
- [74] L.-M. Liu, C.-J. Zhang, J. Zhou, J. Xu, J. Jia, and G.-X. Peng, *Phys. Lett. B* **834**, 137441 (2022).
- [75] Y.-L. Cheng, S. Shi, Y.-G. Ma, H. Stöcker, and K. Zhou, *Phys. Rev. C* **107**, 064909 (2023).
- [76] J. Zhao and S. Shi, *Eur. Phys. J. C* **83**, 511 (2023).
- [77] B. Schenke, C. Shen, and P. Tribedy, *Phys. Rev. C* **99**, 044908 (2019).
- [78] P. Alba, V. Mantovani Sarti, J. Noronha, J. Noronha-Hostler, P. Parotto, I. P. Vazquez, and C. Ratti, *Phys. Rev. C* **98**, 034909 (2018).
- [79] C. Mordasini, A. Bilandzic, D. Karakoç, and S. F. Taghavi, *Phys. Rev. C* **102**, 024907 (2020).
- [80] Z. Moravcova, K. Gulbrandsen, and Y. Zhou, *Phys. Rev. C* **103**, 024913 (2021).
- [81] M. Li, Y. Zhou, W. Zhao, B. Fu, Y. Mou, and H. Song, *Phys. Rev. C* **104**, 024903 (2021).
- [82] A. Bilandzic, M. Lesch, C. Mordasini, and S. F. Taghavi, *Phys. Rev. C* **105**, 024912 (2022).
- [83] G. Nijs and W. van der Schee, *SciPost Phys.* **15**, 041 (2023).
- [84] C. Zhang and J. Jia, *Phys. Rev. Lett.* **128**, 022301 (2022).
- [85] A. Bilandzic, M. Lesch, and S. F. Taghavi, *Phys. Rev. C* **102**, 024910 (2020).
- [86] S. F. Taghavi, *Eur. Phys. J. C* **81**, 652 (2021).
- [87] S. Acharya *et al.* (ALICE Collaboration), *Phys. Lett. B* **773**, 68 (2017).
- [88] Z.-W. Lin, C. M. Ko, B.-A. Li, B. Zhang, and S. Pal, *Phys. Rev. C* **72**, 064901 (2005).
- [89] G.-L. Ma and Z.-W. Lin, *Phys. Rev. C* **93**, 054911 (2016).
- [90] M. R. Haque, M. Nasim, and B. Mohanty, *J. Phys. G* **46**, 085104 (2019).
- [91] P. P. Bhaduri and S. Chattopadhyay, *Phys. Rev. C* **81**, 034906 (2010).
- [92] M. Nasim, L. Kumar, P. K. Netrakanti, and B. Mohanty, *Phys. Rev. C* **82**, 054908 (2010).

- [93] J. Xu and C. M. Ko, *Phys. Rev. C* **83**, 021903(R) (2011).
- [94] N. Magdy, O. Evdokimov, and R. A. Lacey, *J. Phys. G* **48**, 025101 (2021).
- [95] Y. Guo, S. Shi, S. Feng, and J. Liao, *Phys. Lett. B* **798**, 134929 (2019).
- [96] K. Hagino, N. W. Lwin, and M. Yamagami, *Phys. Rev. C* **74**, 017310 (2006).
- [97] P. Moller, J. R. Nix, W. D. Myers, and W. J. Swiatecki, *At. Data Nucl. Data Tables* **59**, 185 (1995).
- [98] B. Zhang, *Comput. Phys. Commun.* **109**, 193 (1998).
- [99] J. Xu and C. M. Ko, *Phys. Rev. C* **83**, 034904 (2011).
- [100] M. Nasim, *Phys. Rev. C* **95**, 034905 (2017).
- [101] X.-N. Wang and M. Gyulassy, *Phys. Rev. D* **44**, 3501 (1991).
- [102] M. Gyulassy and X.-N. Wang, *Comput. Phys. Commun.* **83**, 307 (1994).
- [103] B.-A. Li and C. M. Ko, *Phys. Rev. C* **52**, 2037 (1995).
- [104] A. Bilandzic, R. Snellings, and S. Voloshin, *Phys. Rev. C* **83**, 044913 (2011).
- [105] A. Bilandzic, C. H. Christensen, K. Gulbrandsen, A. Hansen, and Y. Zhou, *Phys. Rev. C* **89**, 064904 (2014).
- [106] K. Gajdošová (ALICE Collaboration), Proceedings of the 26th International Conference on Ultra-relativistic Nucleus-Nucleus Collisions (Quark Matter 2017), Chicago, Illinois, USA, February 5–11, 2017 [*Nucl. Phys. A* **967**, 437 (2017)].
- [107] J. Jia, M. Zhou, and A. Trzupek, *Phys. Rev. C* **96**, 034906 (2017).
- [108] G. Giacalone, J. Noronha-Hostler, and J.-Y. Ollitrault, *Phys. Rev. C* **95**, 054910 (2017).
- [109] G. Giacalone, L. Yan, J. Noronha-Hostler, and J.-Y. Ollitrault, *Phys. Rev. C* **95**, 014913 (2017).
- [110] J. Jia (ATLAS Collaboration), *Nucl. Phys. A* **904–905**, 421c (2013).
- [111] S. A. Voloshin, A. M. Poskanzer, A. Tang, and G. Wang, *Phys. Lett. B* **659**, 537 (2008).
- [112] B. Aboona *et al.* (STAR Collaboration), *Phys. Lett. B* **839**, 137755 (2023).
- [113] R. A. Lacey, Y. Gu, X. Gong, D. Reynolds, N. N. Ajitanand, J. M. Alexander, A. Mwai, and A. Taranenko, [arXiv:1301.0165](https://arxiv.org/abs/1301.0165).
- [114] J. Adam *et al.* (STAR Collaboration), *Phys. Lett. B* **784**, 26 (2018).
- [115] L. Adamczyk *et al.* (STAR Collaboration), *Phys. Rev. C* **88**, 014904 (2013).
- [116] Z. Lu, M. Zhao, X. Li, J. Jia, and Y. Zhou, *Eur. Phys. J. A* **59**, 279 (2023).
- [117] G. Giacalone, J. Jia, and V. Somà, *Phys. Rev. C* **104**, L041903 (2021).
- [118] P. Sinha, V. Bairathi, K. Gopal, C. Jena, and S. Kabana, *Phys. Rev. C* **108**, 024911 (2023).
- [119] H.-J. Xu, *EPJ Web Conf.* **276**, 06020 (2023).